Experimental and theoretical triple-differential cross sections for tetrahydrofuran ionized by low-energy 26-eV-electron impact

Esam Ali,[1] XueGuang Ren,[2] Alexander Dorn,[2] Chuangang Ning,[3] James Colgan,[4] and Don Madison[1]
[1]*Department of Physics, Missouri University of Science and Technology, Rolla, Missouri 65409, USA*
[2]*Max Planck Institut für Kernphysik, Saupfercheckweg 1, 69117 Heidelberg, Germany*
[3]*Department of Physics, State Key Laboratory of Low-Dimensional Quantum Physics, Tsinghua University, Beijing 100084, China*
[4]*Theoretical Division, Los Alamos National Laboratory, Los Alamos, New Mexico 87545, USA*
(Received 16 March 2016; revised manuscript received 28 April 2016; published 13 June 2016)

We report an experimental and theoretical study of low-energy electron-impact ionization of tetrahydrofuran, which is a molecule of biological interest. The experiments were performed using an advanced reaction microscope specially built for electron-impact ionization studies. The theoretical calculations were performed within the molecular three-body distorted-wave model. Reasonably good agreement is found between experiment and theory.

DOI: 10.1103/PhysRevA.93.062705

I. INTRODUCTION

The interactions of electrons with atoms, molecules, and clusters are of great importance in a wide range of scientific and practical applications [1]. For example, in medical radiation therapy, it has been discovered that significant damage to DNA is induced by electrons with energies below 100 eV [2,3], which are the most abundant secondary species in media penetrated by high-energy ionizing radiation [4]. Even slow electrons with energies below the ionization threshold ($\leqslant$10 eV) can produce considerable DNA strand breaks via dissociative electron attachment resonances. Above this energy range the damage to DNA is dominated by a superposition of various nonresonant mechanisms related to excitation, ionization, and dissociation. Therefore, a number of experimental and theoretical works examining electron interactions with biomolecules have been carried out to study the dynamics of electrons in biological media, see, e.g., [5–13]. Here, tetrahydrofuran (THF, C_4H_8O) has been used frequently since it is one of the simplest molecular analogs of the DNA bases.

A comprehensive way to characterize the dynamics of electron-impact ionization of matter is to detect the two outgoing electrons in coincidence, the so-called (e, 2e) method, which serves as a powerful tool to understand the electron trajectory in a media. This is a kinematically complete experiment in which the linear momentum vectors of all final-state particles are determined. The quantity measured in such experiments is the triple-differential cross section (TDCS), i.e., a cross section that is differential in the solid angles of both electrons and the energy of one of them (energy conservation determines the energy of the second electron). Such (e, 2e) experiments for THF have been recently performed at high collision energy (250 eV) [14]. In the present work, we study low-energy ($E_0 = 26.5$ eV) electron-impact ionization of THF to understand the features of low-energy electrons in biological systems using the kinematically complete (e,2e) experiments. For low-energy electrons, the effects of postcollision interaction (PCI), electron exchange, and electron-target interactions are expected to become more pronounced, which might significantly influence the electron trajectory in matter [14,15]. The TDCSs were measured for an ejected electron energy of 3.5 eV for a range of projectile scattering angles ($\theta_a = 15^\circ$, 25°, and 35°) and resolving different fragmentation channels ($C_4H_8O^+$,$C_4H_7O^+$, and $C_3H_6{}^+$). The experimental data were compared with theoretical predictions from the distorted-wave Born approximation (DWBA) with inclusion of the postcollision interaction (PCI) using the Ward-Macek method [16] and the molecular three-body distorted-wave (M3DW) approach (see, e.g., [17,18]).

II. EXPERIMENTAL METHODS

The experiment was performed using an advanced reaction microscope specially built for electron-impact ionization studies [19]. Details of the setup were described elsewhere [20]. A brief outline will be given here. A well-focused ($\sim$1 mm diameter), pulsed electron beam crosses a supersonic gas jet with internal temperature of $T \sim 10$ K. It is produced by supersonic gas expansion from a 30-μm nozzle and two-stage differential pumping system. Here, helium gas with a partial pressure of 2 bar mixed with THF with a partial pressure of 500 mbar was used. The pulsed electron beam is emitted from a recently developed photoemission electron gun ($\Delta E < 0.5$ eV) in which a pulsed ultraviolet laser beam ($\lambda =$ 266 nm, $\Delta t < 0.5$ ns) illuminates a tantalum photocathode. The projectile beam axis (defining the longitudinal direction) is adjusted parallel to the electric and magnetic extraction fields, which are used to guide electrons and ions onto two position- and time-sensitive multihit detectors equipped with fast delay-line readout.

Experimental data were measured using the triple coincidences method in which both outgoing electrons (the faster electron E_a and the slower electron E_b) and the fragment ion are recorded. From the positions of the hits and the times of flight, the vector momenta of the detected particles can be determined. Note that the projectile beam is adjusted exactly parallel to the electric and magnetic extraction fields. After passing through the target gas jet, the beam arrives at the electron detector, where a central hole in the multichannel plates allows for the undeflected electrons to pass without inducing a hit. The detection solid angle for electrons is close to 4π, apart from the acceptance holes at small forward and backward angles where the electrons end up in the

detector bore. In the fragmentation processes of molecules, the dissociated ions are usually created with some kinetic energy. In order to cover a large solid angle for the detection of the fragment ions, a pulsed electric field has been applied for ion extraction. In this way, significantly improved mass and energy resolutions have been achieved [20,21].

III. THEORETICAL METHODS

In this paper, we have used the M3DW approach which is described in Refs. [22–24]. For the three-body problem, the TDCS, which we evaluate numerically, is given by

$$\frac{d^5\sigma}{d\Omega_a d\Omega_b dE_b} = \frac{1}{(2\pi)^5}\frac{k_a k_b}{k_i}(|T_{\rm dir}|^2+|T_{\rm exc}|^2+|T_{\rm dir}-T_{\rm exc}|^2), \tag{1}$$

where $T_{\rm dir}$ and $T_{\rm exc}$ are the direct and exchange scattering amplitudes. The direct amplitude is given by

$$T_{\rm dir} = \langle \chi_a^-(\mathbf{k}_a,\mathbf{r}_0)\chi_b^-(\mathbf{k}_b,\mathbf{r}_1)C_{ab}(\mathbf{r}_{01})|W|\phi_{Dy}^{OA}(\mathbf{r}_1)\chi_i^+(\mathbf{k}_i,\mathbf{r}_0)\rangle. \tag{2}$$

Here $\chi_i^+(\mathbf{k}_i,\mathbf{r}_0)$ is an initial-state distorted wave for the incoming electron with wave number $\mathbf{k}_i$ and the $(+)$ indicates outgoing wave boundary conditions; $\chi_a^-(\mathbf{k}_a,\mathbf{r}_0)$ and $\chi_b^-(\mathbf{k}_b,\mathbf{r}_1)$ are the final-state distorted wave functions for the faster and slower electrons with wave numbers, $\mathbf{k}_a$ and $\mathbf{k}_b$, respectively, the $(-)$ indicating incoming wave boundary conditions. We, of course, do not know which electron is the scattered projectile and which electron is the ejected electron, but for discussion purposes, we call the faster electron the scattered electron and the slower electron the ejected electron. The perturbation $W = V_i - U_i$, where V_i is the initial-state interaction between the projectile and neutral target, and U_i is a spherically symmetric approximation for V_i. $\phi_{Dy}^{OA}(\mathbf{r}_1)$ is an initial bound-state Dyson molecular orbital averaged over all orientations [24] and $\mathbf{r}_1$ is the active electron coordinate. $C_{ab}(\mathbf{r}_{01})$ is the Coulomb interaction between the projectile and ejected electron [normally called the postcollision interaction (PCI)], which can be expressed as

$$C_{ab}(\mathbf{r}_{01}) = e^{\frac{-\pi\gamma}{2}}\Gamma(1-i\gamma)\,{}_1F_1[i\gamma,1,-i(k_{ab}r_{01}+\mathbf{k}_{ab}\cdot\mathbf{r}_{01})]. \tag{3}$$

Here Γ is the gamma function, $\mathbf{k}_{ab} = \mu\mathbf{v}_{ab}$ is the relative electron-electron wave number, which depends on the relative velocity $\mathbf{v}_{ab}$ and the reduced mass for the two electrons μ, ${}_1F_1$ is a confluent hypergeometric function, and γ is the Somerfield parameter ($\gamma = 1/\mathbf{v}_{ab}$). In the Ward-Macek approximation [16], one replaces the actual final-state electron-electron separation $\mathbf{r}_{01}$ by an average value directed parallel to $\mathbf{k}_{ab}$. The average separation is defined as

$$r_{01}^{\rm ave} = \frac{\pi^2}{16\varepsilon_t}\left(1+\frac{0.627}{\pi}\sqrt{\varepsilon_t}\ln\varepsilon_t\right)^2, \tag{4}$$

where ε_t is the total energy of the scattered and ejected electrons. In the Ward-Macek approximation, PCI is approximated as

$$C_{ab}\left(r_{01}^{\rm ave}\right) = e^{\frac{-\pi\gamma}{2}}\Gamma(1-i\gamma)\,{}_1F_1\left(i\gamma,1,-2ik_{ab}\,r_{01}^{\rm ave}\right), \tag{5}$$

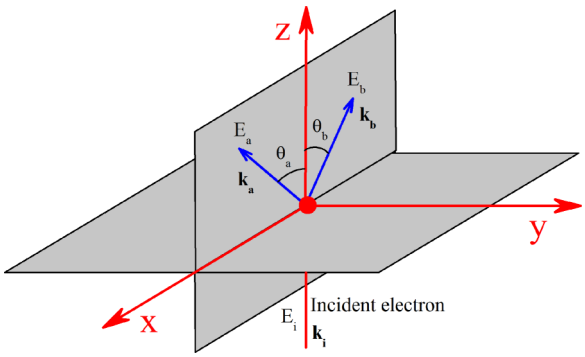

FIG. 1. Schematic diagram of coplanar geometry.

which does not depend on electron coordinates and can be removed from the integral in the T matrix. With the PCI term removed from the integral, the T matrix becomes the standard DWBA. We will label results using the Ward-Macek approximation for PCI as WM and results using the exact PCI of Eq. (3) as M3DW. The only difference between the two calculations is the treatment of PCI. The exchange amplitude $T_{\rm exc}$ is the same as Eq. (2), with $\mathbf{r}_0$ and $\mathbf{r}_1$ interchanged in the final-state wave function.

IV. RESULTS

A schematic diagram of the geometry for coplanar scattering is presented in Fig. 1 where the scattering plane is the xz plane. Here we will present results for $E_0 = 26.5\,\text{eV}, E_b = 3.5\,\text{eV}$, faster final-state electron scattering angles $\theta_a = 15°$, $25°$, and $35°$, and ejected electron angles θ_b ranging from 0° to 360° measured clockwise.

In the experiment, the scattered and ejected electrons are measured in coincidence with one fragment ion. The detected

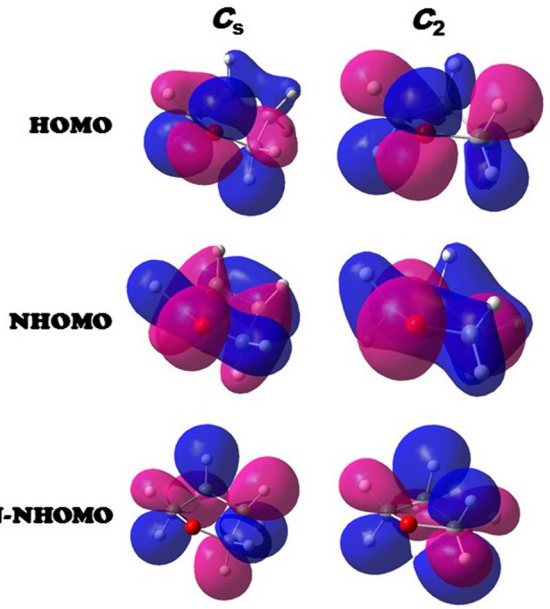

FIG. 2. THF conformers C_s and C_2 for the HOMO, NHOMO, and N-NHOMO states.

cations are $C_4H_8O^+$, $C_4H_7O^+$, and $C_3H_6^+$. It has been identified in Ref. [20] that the cation $C_4H_8O^+$ is attributed to the ionization of 9b, i.e., the highest occupied molecular orbital (HOMO) of THF, and the cation $C_4H_7O^+$ is attributed to the ionization of the 9b (20%) and 11a orbital (80%) (the next highest occupied molecular orbital "NHOMO") of THF. The most abundant ion in the fragmentation of THF has been identified as the $C_3H_6^+$ fragment, which is attributed to the ionization of the 11a (12%), 10a (46%) (next-next highest occupied molecular orbital "N-NHOMO"), 8b (21%), and 9a (21%) orbitals of THF. There are two conformers for THF labeled C_s and C_2 and the above weights are for C_2. Figure 2 shows the two conformers for HOMO, NHOMO, and N-NHOMO which make the dominant contributions to the three measured cations. For the theoretical calculations, the TDCS for the two conformers are summed using the ratios $55\%C_s+45\%C_2$ [25,26]. Figures 3–5 show the calculated conformer cross sections for the three measured cations in atomic units. As is seen, the two cross sections are very similar so the conformer weights are relatively unimportant.

Figure 6 compares theoretical and experimental results for ionization of the THF HOMO (ionization energy of 9.7 eV) state which leads to the $C_4H_8O^+$ cation. Since the ratios of the experimental data for different angles and different ionized

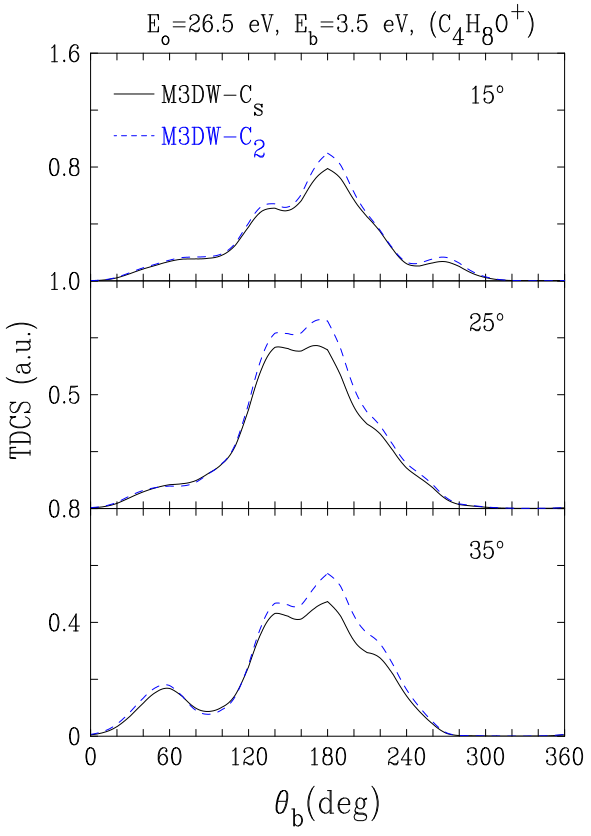

FIG. 3. Theoretical TDCS in atomic units for 26.5-eV electron-impact ionization of the THF HOMO state which leads to the cation $C_4H_8O^+$ as a function of the ejected electron scattering angle θ_b. The faster electron scattering angle is θ_a is indicated in each panel. The solid (black) lines are the M3DW results for the C_s conformer, and dashed (blue) lines are the M3DW results for the C_2 conformer.

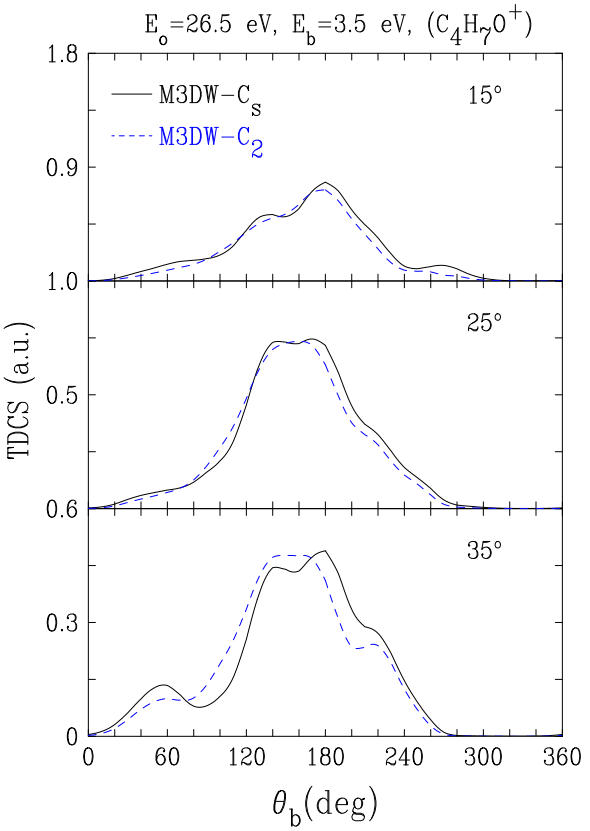

FIG. 4. Theoretical TDCS in atomic units for 26.5-eV electron-impact ionization of the THF combination of states which leads to the cation $C_4H_7O^+$ as a function of the ejected electron scattering angle θ_b. The faster electron scattering angle is θ_a is indicated in each panel. The solid (black) lines are the M3DW results for the C_s conformer, and dashed (blue) lines are the M3DW results for the C_2 conformer.

orbitals are absolute, the experiment has been normalized to theory using a single normalization factor for all scattering angles and the three measured states. This normalization factor was chosen for best visual fit of experimental and M3DW cross sections for ionization of the THF HOMO state and $\theta_a = 15°$ (Fig. 6, top panel). Both theories are absolute (in atomic units) with no normalization. The solid (red) curves are the results of the M3DW calculation, and the dashed (blue) curves are the results using the WM approximation for PCI. Overall, the M3DW results are in better agreement with experiment than the WM, although the WM does predict the experimental dip seen near 160° for $\theta_a = 25°$ and 35°. The M3DW predicts the shape of the data much better for small projectile scattering angles and small ejected electron angles. From studies of electron-impact ionization of atoms, it has been found that the typical (e,2e) coplanar cross sections have a large peak in the forward direction. This peak is called the classical binary peak since it is close to the direction that a classical particle would leave a collision for elastic scattering of two equal mass particles (the momentum transfer direction $+\mathbf{q}$). Also, typically there is a much smaller peak at large angles, which is normally close to 180° from the binary peak (the negative of the momentum transfer direction $-\mathbf{q}$), and this small peak is called the recoil peak since it is attributed

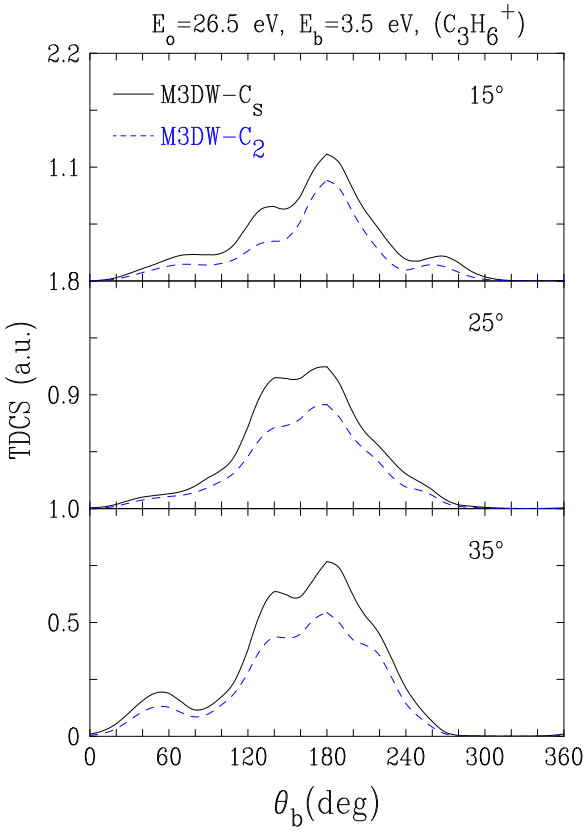

FIG. 5. Theoretical TDCS in atomic units for 26.5-eV electron-impact ionization of the THF combination of states which leads to the cation $C_3H_6^+$ as a function of the ejected electron scattering angle θ_b. The faster electron scattering angle θ_a is indicated in each panel. The solid (black) lines are the M3DW results for the C_s conformer, and dashed (blue) lines are the M3DW results for the C_2 conformer.

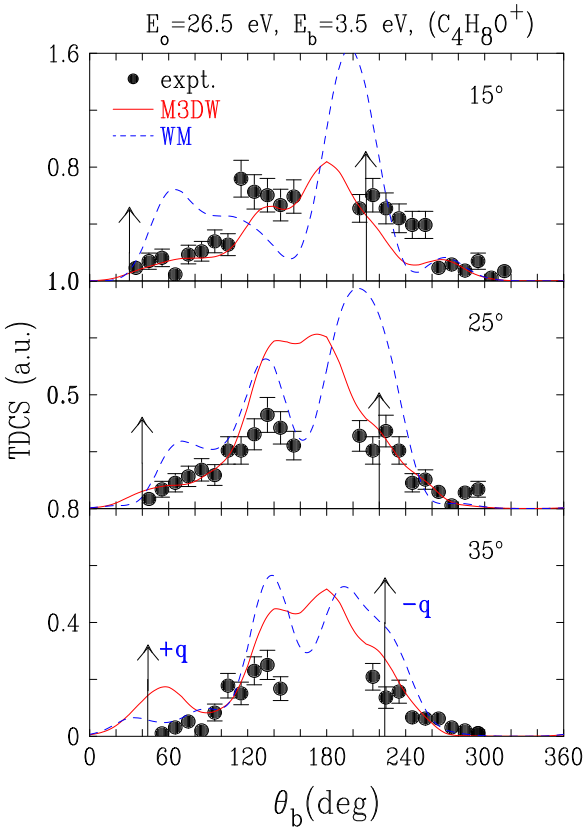

FIG. 6. Experimental and theoretical TDCS in atomic units for 26.5-eV-electron impact ionization of the THF HOMO state, which leads to the cation $C_4H_8O^+$ as a function of the ejected electron scattering angle θ_b. The faster electron scattering angle θ_a is indicated in each panel. The experimental data are the circles, the solid (red) lines are the M3DW results, and the dashed (blue) lines are the WM results. The theoretical results are in atomic units, and one normalization factor for experiment has been used for all panels of Figs. 6–8.

to a binary electron being backscattered from the nucleus. The location of these two directions is shown by the vertical arrows in the figure. It is seen that the experimental data shows no indication of a binary peak but possibly a recoil peak. The WM approximation has a peak near the binary direction but shifted to larger angles and a peak near the recoil direction but shifted to smaller angles. Angular shifts like this would normally be attributed to PCI repulsion, but we think that this is an unlikely explanation since WM has PCI only to first order and the shifts are bigger than one would expect to first order. Similar to the experimental data, M3DW has no peaks in the binary region for the two smaller projectile scattering angles and a small peak at the largest angle. The experimental data also has a small hint of a binary-type peak for $\theta_a = 35°$. The M3DW also has a large angle peak at considerably smaller angles than the expected recoil direction. What is very clear is that these cross sections do not have the standard two-peak binary and recoil structure normally found in atomic ionization. Consequently, it appears that the shape of the TDCS for these more complicated multicenter targets and at the present low impact energy probably cannot be explained by simple classical models.

Figure 7 compares experimental and theoretical results for ionization of the combination of THF states which lead to the $C_4H_7O^+$ cation. The comparison between theory and experiment is similar to the HOMO state. For this case the M3DW is again in better overall agreement with experiment. The WM results predict a peak near the recoil direction that is much larger than experiment, especially for the smaller projectile scattering angles. The agreement between experiment and the M3DW is very good for the smallest projectile scattering angle. Although qualitatively similar, the agreement with experiment for the 35° projectile scattering angle is not as good as it was for the HOMO state. Figure 8 compares experimental and theoretical results for ionization of the combination of THF states which lead to the $C_3H_6^+$ cation and again the results are similar to the previous two states. However, for this case, the agreement of M3DW with the 25° and 35° data is better than for the other two states. Interestingly, the WM results are in quite good agreement with the 25° data for all three cases. Overall the theoretical cross sections are highest in the vicinity of $\theta_b = 180°$, which is in accordance with the strong PCI effects present for two outgoing electrons with low energies ($E_a = 10$–13 eV, $E_b = 3.5$ eV) and the resulting preferred back-to-back emission of both electrons.

It is interesting to note that the cross-section patterns are not particularly sensitive to the specific initial orbital being

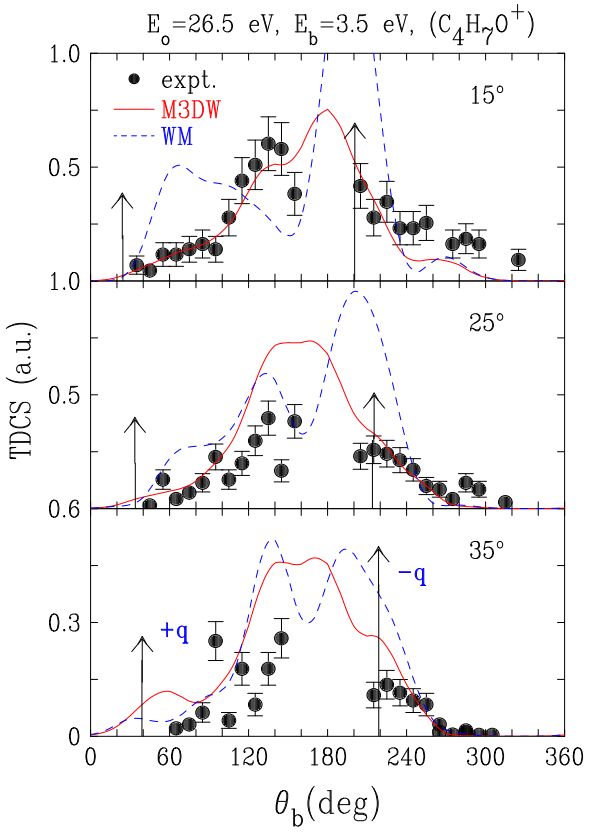

FIG. 7. Experimental and theoretical TDCS in atomic units for 26.5-eV-electron impact ionization of the combination of THF states which leads to the cation $C_4H_7O^+$ as a function of the ejected electron scattering angle θ_b. The faster electron scattering angle θ_a is indicated in each panel. The experimental data are the circles, the solid (red) lines are the M3DW results, and the dashed (blue) lines are the WM results. The theoretical results are in atomic units, and one normalization factor for experiment has been used for all panels of Figs. 6–8.

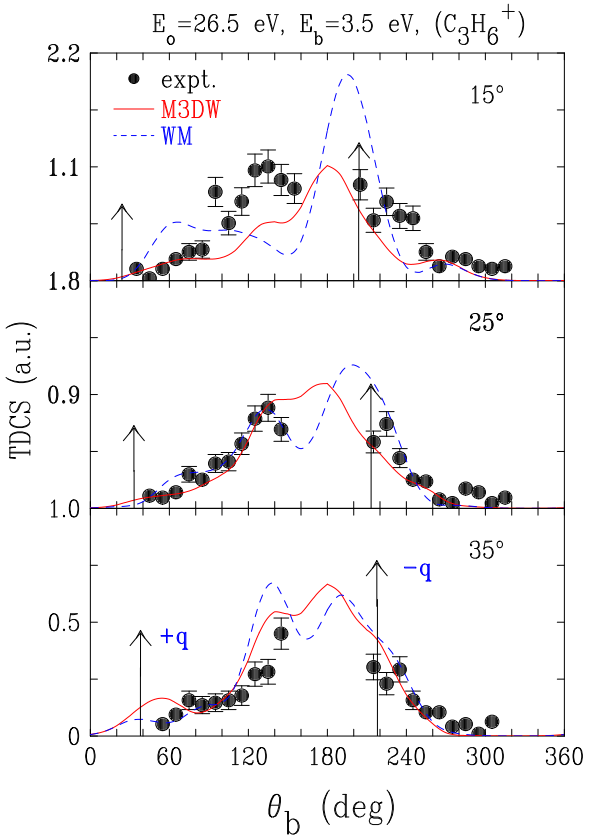

FIG. 8. Experimental and theoretical TDCS in atomic units for 26.5-eV-electron impact ionization of the combination of THF states, which leads to the cation $C_3H_6^+$ as a function of the ejected electron scattering angle θ_b. The faster electron scattering angle θ_a is indicated in each panel. The experimental data are the circles, the solid (red) lines are the M3DW results, and the dashed (blue) lines are the WM results. The theoretical results are in atomic units, and one normalization factor for experiment has been used for all panels of Figs. 6–8.

ionized. This is also the case for the two THF conformers C_s and C_2, which show essentially identical TDCS as was shown in Figs. 3–5. This may seem surprising since the orbital spatial structures differ greatly (Fig. 2), even belonging to different symmetries. Nevertheless, their orbital momentum distributions (MDs) are rather similar if the molecular alignment is not resolved. The spherically averaged MDs for various orbitals of THF have been measured by Ning *et al.* [26]. We are concerned with the MD of the HOMO (binding energy 9.7 eV) and a group involving the NHOMO and N-NHOMO orbitals (up to 12-eV binding energy). Both MDs are very similar. They range from zero up to about 2 a.u. with two maxima in that range which are only slightly differently positioned in both cases. Thus, the effect of the MD of the initially bound electron which is present in the momentum and angular distributions of the ejected electron will be similar for these orbitals. In addition, the spatial charge-density distributions of all these orbitals are spread out over the whole molecule, as can be seen in Fig. 2. Thus, the resulting multicenter potential of the singly charged ion which is experienced by the outgoing electrons will not be strongly different for ionization of the various orbitals. Consequently, rescattering processes in the ionic potential which give rise, e.g., to the typical recoil peak observed in the (e,2e) studies at higher energies should also be similar for the different orbitals. As a result, it is perhaps not so surprising that we have found no large variation in the electron emission pattern for the different orbitals.

V. CONCLUSIONS

In summary, we have measured relatively absolute cross sections for ionization of THF states which lead to three different cations. This means that there is only one normalization factor used for the experiment for all three states and all three projectile scattering angles (nine panels in all). We have found reasonably good agreement between experiment and theory (both shape and magnitude) for the final-state cations $C_4H_8O^+$, $C_4H_7O^+$, and $C_3H_6^+$ of THF for a relatively low incident electron energy of 26.5 eV. Although there is considerable structure in the measured and calculated cross sections, they do not have the traditional binary and recoil peaks, which is not surprising considering the complicated multicenter scattering centers for a large molecule such as this. Overall the M3DW is in fairly good agreement, both

in magnitude and shape, with all the measured states and scattering angles. These results indicate that the theoretical M3DW TDCS could be reliably used in the track structure modeling calculations for biological media.

ACKNOWLEDGMENTS

E.A. and D.M. would like to acknowledge the support of the U.S. National Science Foundation under Grant No. PHY-1505819, and C.N. would like to acknowledge the support of the National Natural Science Foundation of China under Grant No. 11174175. Computational work was performed with institutional computing resources made available through the Los Alamos National Laboratory. The Los Alamos National Laboratory is operated by Los Alamos National Security, LLC, for the National Nuclear Security Administration of the U.S. Department of Energy under Contract No. DE-AC5206NA25396.

[1] B. C. Garrett *et al.*, Chem. Rev. **105**, 355 (2005).
[2] M. A. Huels, B. Boudaiffa, P. Cloutier, D. Hunting, and L. Sanche, J. Am. Chem. Soc. **125**, 4467 (2003).
[3] E. Alizadeh, T. M. Orlando, and L. Sanche, Ann. Rev. Phys. Chem. **66**, 379 (2015).
[4] S. M. Pimblott and J. A. LaVerne, Radiat. Phys. Chem. **76**, 1244 (2007).
[5] M. Fuss, A. Muñoz, J. C. Oller, F. Blanco, D. Almeida, P. Limão Vieira, T. P. D. Do, M. J. Brunger, and G. Garcia, Phys. Rev. A **80**, 052709 (2009).
[6] A. Zecca, C. Perazzolli, and M. J. Brunger, J. Phys. B **38**, 2079 (2005).
[7] P. Mozejko, E. Ptasinska-Denga, A. Domaracka, and C. Szmytkowski, Phys. Rev. A **74**, 012708 (2006).
[8] W. Y. Baek, M. Bug, H. Rabus, E. Gargioni, and B. Grosswendt, Phys. Rev. A **86**, 032702 (2012).
[9] L. Chiari, E. Anderson, W. Tattersall, J. R. Machacek, P. Palihawadana, C. Makochekanwa, J. P. Sullivan, G. Garcia, F. Blanco, R. P. McEachran, M. J. Brunger, and S. J. Buckman, J. Chem. Phys. **138**, 074301 (2013).
[10] M. Allan, J. Phys. B **40**, 3531 (2007).
[11] C. J. Colyer, V. Vizcaino, J. P. Sullivan, M. J. Brunger, and S. J. Buckman, New J. Phys. **9**, 41 (2007).
[12] M. Dampc, A. R. Milosavljevic, I. Linert, B. P. Marinkovic, and M. Zubek, Phys. Rev. A **75**, 042710 (2007).
[13] A. Gauf, L. R. Hargreaves, A. Jo, J. Tanner, M. A. Khakoo, T. Walls, C. Winstead, and V. McKoy, Phys. Rev. A **85**, 052717 (2012).
[14] J. D. Builth-Williams, S. M. Bellm, L. Chiari, P. A. Thorn, D. B. Jones, H. Chaluvadi, D. H. Madison, C. G. Ning, B. Lohmann, G. B. da Silva, and M. J. Brunger, J. Chem. Phys. **139**, 034306 (2013).
[15] X. Ren, S. Amami, O. Zatsarinny, T. Pfluger, M. Weyland, W. Y. Baek, H. Rabus, K. Bartschat, D. Madison, and A. Dorn, Phys. Rev. A **91**, 032707 (2015).
[16] S. J. Ward and J. H. Macek, Phys. Rev. A **49**, 1049 (1994).
[17] O. Al-Hagan, C. Kaiser, A. J. Murray, and D. Madison, Nat. Phys. **5**, 59 (2009).
[18] O. Al-Hagan, A. J. Murray, C. Kaiser, J. Colgan, and D. H. Madison, Phys. Rev. A **81**, 030701 (2010).
[19] J. Ullrich, R. Moshammer, A. Dorn, R. Doerner, L. Schmidt, and H. Schmidt-Boecking, Rep. Prog. Phys. **66**, 1463 (2003).
[20] X. Ren, T. Pflueger, M. Weyland, W. Y. Baek, H. Rabus, J. Ullrich, and A. Dorn, J. Chem. Phys. **141**, 134314 (2014).
[21] X. Ren, T. Pflueger, M. Weyland, W. Y. Baek, H. Rabus, J. Ullrich, and A. Dorn, J. Chem. Phys. **142**, 174313 (2015).
[22] J. Gao, D. H. Madison, and J. L. Peacher, J. Chem. Phys. **123**, 204314 (2005).
[23] J. Gao, D. H. Madison, and J. L. Peacher, Phys. Rev. A **72**, 032721 (2005).
[24] J. Gao, D. H. Madison, and J. L. Peacher, J. Chem. Phys. **123**, 204302 (2005).
[25] Tiecheng Yang, Guolin Su, Chuangang Ning, Jingkang Deng, Feng Wang, Shufeng Zhang, Xueguang Ren, and Yanru Huang, J. Phys. Chem. A **111**, 4927 (2007).
[26] C. G. Ning, Y. R. Huang, S. F. Zhang, J. K. Deng, K. Liu, Z. H. Luo, and F. Wang, J. Phys. Chem. A **112**, 11078 (2008).